Mineralization of organic pollutants by anodic oxidation using reactive electrochemical membrane synthesized from carbothermal reduction of TiO_2

Clément Trellu [a, *], Clémence Coetsier [a], Jean-Christophe Rouch [a], Roseline Esmilaire [b], Matthieu Rivallin [b], Marc Cretin [b], Christel Causserand [a]

[a] Laboratoire de Génie Chimique, Université de Toulouse, CNRS, INPT, UPS, Toulouse, France
[b] Institut Européen des Membranes, UMR 5635 (CNRS-ENSCM-UM), Montpellier, France

A B S T R A C T

Reactive Electrochemical Membrane (REM) prepared from carbothermal reduction of TiO_2 is used for the mineralization of biorefractory pollutants during filtration operation. The mixture of Ti_4O_7 and Ti_5O_9 Magnéli phases ensures the high reactivity of the membrane for organic compound oxidation through $^{\bullet}OH$ mediated oxidation and direct electron transfer. In cross-flow filtration mode, convection-enhanced mass transport of pollutants can be achieved from the high membrane permeability (3300 LMH bar^{-1}). Mineralization efficiency of oxalic acid, paracetamol and phenol was assessed as regards to current density, transmembrane pressure and feed concentration. Unprecedented high removal rates of total organic carbon and mineralization current efficiency were achieved after a single passage through the REM, e.g. 47 g m^{-2} h^{-1} – 72% and 6.7 g m^{-2} h^{-1} – 47% for oxalic acid and paracetamol, respectively, at 15 mA cm^{-2}. However, two mechanisms have to be considered for optimization of the process. When the TOC flux is too high with respect to the current density, aromatic compounds polymerize in the REM layer where only direct electron transfer occurs. This phenomenon decreases the oxidation efficiency and/or increases REM fouling. Besides, O_2 bubbles sweeping at high permeate flux promotes O_2 gas generation, with adverse effect on oxidation efficiency.

1. Introduction

Anodic oxidation (AO) is an electrochemical advanced oxidation process (EAOP) increasingly recognized as a promising next-generation technology for the treatment of contaminated effluents (Panizza and Cerisola, 2009; Chaplin, 2014; Radjenovic and Sedlak, 2015; Moreira et al., 2017). The process is based on both direct electron transfer (DET) from organic compounds (R) to the anode surface (eq. (1)) and generation of hydroxyl radicals ($^{\bullet}OH$) from water oxidation on the surface of electrodes (M) with high O_2 overvoltage (eq. (2)) (Panizza and Cerisola, 2009). $^{\bullet}OH$ is a very strong oxidant ($E^{\circ} = 2.8$ V *vs* SHE) (Latimer, 1952) allowing the degradation of a large range of bio-refractory organic compounds. Mineralization of various micropollutants and complex effluents has been achieved using AO (Özcan et al., 2008; Balci et al., 2009; Oturan et al., 2015; Martínez-Huitle et al., 2015; Brillas and Martínez-Huitle, 2015; Antonin et al., 2015; Trellu et al., 2016). However, several scientific challenges still need to be overcome in order to promote the application of AO for water treatment.

$$R \rightarrow (R^{\bullet})^{+} + e^{-} \quad (1)$$

$$M + H_2O \rightarrow M(^{\bullet}OH) + H^{+} + e^{-} \quad (2)$$

$^{\bullet}OH$ are produced in a heterogeneous way in the electrochemical cell, therefore, new approaches are necessary in order to break the high cost bottleneck related to the limited mass transfer of organic pollutants from the bulk to the electrode surface (Yang et al., 2009; Chaplin, 2014; Radjenovic and Sedlak, 2015). Electro-oxidation is controlled by mass transport phenomenon when the concentration of organic compounds is too low by comparison to the electron transfer rate (current density). In the potential region of water discharge, secondary reactions such as oxygen evolution

* Corresponding author.
E-mail address: cl.trellu@gmail.com (C. Trellu).

strongly decreases the current efficiency (Panizza et al., 2001; Panizza and Cerisola, 2009). Unfortunately, most of anode materials used in AO can only be produced under the form of conventional plate electrodes (e.g. boron-doped diamond), for which mass transport is limited by surface diffusivity in the external film (Brillas and Martínez-Huitle, 2011). This technological constraint also limits the potential for scaling up. Implementation of flow-through porous electrodes is the most promising way to overcome mass transfer limitations (Zaky and Chaplin, 2013; Ganiyu et al., 2015; Radjenovic and Sedlak, 2015; Ronen et al., 2016).

Recently, carbon nanotube electrochemical filters have been developed for the removal of organic pollutants, however they are not active for •OH production (Tsierkezos and Ritter, 2012; Schnoor and Vecitis, 2013; Gao and Vecitis, 2013; Liu et al., 2015). Besides, research works from Guo et al. (2016) showed that a convection-enhanced rate constant for $Fe(CN)_6^{4-}$ oxidation of 1.4 10^{-4} m s^{-1} – the highest reported in the literature, close to the kinetic limit – was reached by using porous sub-stoichiometric titanium oxide (TiO_x) reactive electrochemical membrane (REM) (Guo et al., 2016). The high membrane permeability (3200 L m^{-2} h^{-1} bar^{-1}) resulted in a strong increase of the convective mass transport of pollutants from the bulk solution to electron-transfer sites at the surface and in the porosity of the material. The reactivity of the material has been investigated by using probe molecules (oxalic acid, coumarin, terephthalic acid) showing that both DET and formation of •OH were involved in the oxidation of organic compounds (Zaky and Chaplin, 2013, 2014; Ganiyu et al., 2016). First studies on TiO_x REM used either commercial Ebonex® membranes (Walsh and Wills, 2010; Zaky and Chaplin, 2013) or TiO_2 ultrafiltration membranes reduced to Ti_4O_7 under 1 atm H_2 during 50 h at 1050 °C (Guo et al., 2016). The latter showed the most promising results because of a higher permeability and predominance of the Ti_4O_7 phase but high production costs are associated to the synthesis method.

The focus of this study is on testing a novel TiO_x REM synthesized from carbothermal reduction of TiO_2. The REM is characterized by scanning electron microscopy (SEM), X-ray diffraction (XRD), Hg porosimetry and water permeability. In cross-flow filtration mode, the effect of permeate flux, pollutant concentration and current density on mineralization efficiency of various organic compounds (oxalic acid (OA), paracetamol (PCT), phenol (PHE)) is assessed. A focus is given on phenomena limiting the efficiency of the REM during treatment of aromatic molecules at high concentration or high permeate flux. From the different behaviors observed, electro-oxidation mechanisms and potential of the REM to be applied for water treatment are highlighted.

2. Materials and methods

2.1. Chemicals

All chemicals were of reagent grade and purchased from Sigma Aldrich (Na_2SO_4, PCT, OA) or Alfa Aesar (PHE). Solutions were prepared using ultrapure water (Purelab®, Elga LabWater, 18.2 MΩ cm).

2.2. REM synthesis and characterization

Porous Magneli phase was synthesized from carbothermal reduction of TiO_2 by using an extrusion die, based on the method developed by Saint-Gobain CREE. The extrusion paste contained 74.1% of anatase form of TiO_2 (Altichem, median particle diameter of 0.37 μm), 2.5% of carbon black (Thermax N990), 18.4% of water and 4.9% of organic binders used as extrusion adjuvant. Organic binders were removed during the debinding step under air atmosphere at 350 °C, 2 h. Finally, sintering and carbothermal reduction of TiO_2 to TiO_x was performed during 2 h under argon atmosphere at 1300 °C.

REM morphology was analyzed from images obtained by SEM at high resolution (Hitachi S4800) at 30 and 3000 magnification. Hg porosimetry analysis was performed on a AutoPore IV (Micrometrics) device. The nature of Magneli phases was characterized by powder XRD using X'Pert Pro (Pan Analytical) system with a Cu X-ray tube (40 kV and 20 mA). Scans were collected by Pan Alytical software and processed with Full Prof and Origin Pro software.

2.3. Cross-flow filtration and electro-oxidation setup

The REM (inner and outer diameter of 6 and 10 mm, active length of 9 cm) was used as anode in inside-outside cross-flow filtration mode. A 3 mm diameter stainless steel rod used as cathode was placed at the center of the REM. A recirculating pump and a pressurized reservoir tank ensured constant cross-flow rate (0.88 m s^{-1}) and transmembrane pressure (TMP, 40–1000 mbar). Experiments were performed with OA (0.75–36 mM; TOC = 18–870 mg L^{-1}), PCT (0.1–2.3 mM; TOC = 9.6–220 mg L^{-1}) or PHE (0.25–2 mM; TOC = 18–140 mg L^{-1}) as model organic compounds. Initial pH of the solution was not adjusted and the evolution of the pH in the permeate and retentate was monitored. Sodium sulfate (50 mM) was added as supporting electrolyte. Only the retentate was 100% recirculated, while the permeate was continuously sampled for analysis. Experiments were performed in galvanostatic mode, using a power supply from ELC (AL924A). Current density (j) was in the range 6–30 mA cm^{-2}. Potential difference in the electrochemical cell was in the range 4.0–6.5 V, according to current intensity. All experiments were performed with a constant volume of permeate collected (350 mL). A schematic view of the setup is provided in Fig. 1.

2.4. Analytical methods

Concentration of PCT was analyzed by HPLC (Agilent 1200) with a C18 column and a UV detector (λ = 254 nm). The mobile phase was a mixture of water (with 0.1% formic acid) and acetonitrile (with 0.1% formic acid). HPLC was operated using a constant flow of 1.2 mL min^{-1} and gradient elution (0–3.5 min: 2.5% acetonitrile; 6.5 min: 80% acetonitrile; 7.5–10.5 min: 2.5% acetonitrile). The total organic carbon (TOC) was measured with a Shimadzu TOC-L analyzer using the 680 °C combustion catalytic oxidation method. The relative standard deviation on TOC measurements is 2%.

2.5. Kinetic analysis and figures of merit

Different performance indicators were used for the determination of the oxidation efficiency. The TOC flux, percentage of removal (PR), removal rate (RR) and mineralization current efficiency (MCE, percentage of current directed towards the mineralization of the substrate passing through the REM) of the substrate *i* (molecule or TOC) were calculated as follows (Brillas et al., 2009; Garcia-Segura and Brillas, 2011; Zaky and Chaplin, 2013):

$$TOC\ flux = TOC_f \times J \quad (3)$$

$$PR_i = \frac{\left(C_{f,i} - C_{p,i}\right)}{C_{f,i}} \times 100 \quad (4)$$

$$RR_i = \left(C_{f,i} - C_{p,i}\right) \times J \quad (5)$$

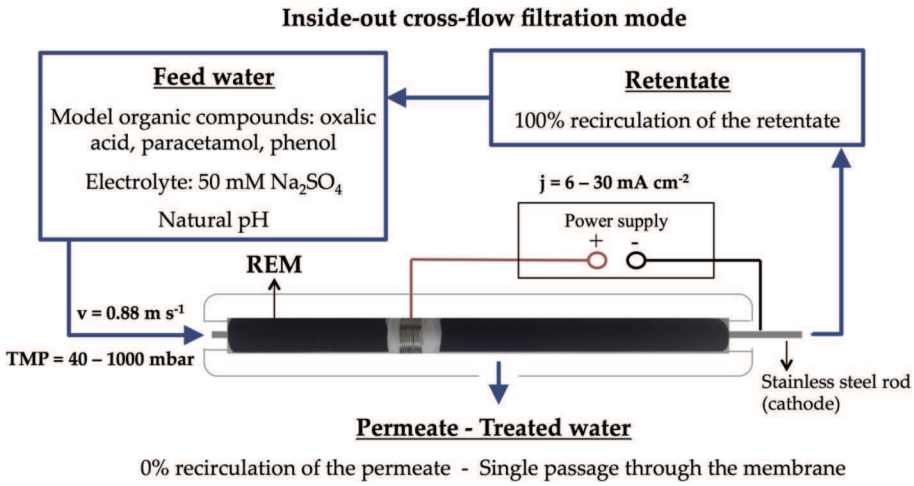

Fig. 1. Schematic view of the combined electro-oxidation/filtration setup.

$$MCE = \frac{n\,F\,J\left(TOC_f - TOC_p\right)}{4.32\times10^7\,m\,j}\times 100 \quad (6)$$

where $C_{f,i}$ and $C_{p,i}$ are the concentration of the feed and permeate (g L^{-1}), J is the permeate flux (L h^{-1} m^{-2}), n is the number of electrons consumed per molecule of substrate mineralized, F is the Faraday constant, 4.32×10^7 is a conversion factor (3600 s h^{-1} × 12,000 mg mol^{-1}), m is the number of carbon atoms of the substrate studied, j is the current density (A m^{-2}) and TOC_f and TOC_p are TOC of the feed and permeate (mg L^{-1}), respectively.

As explained in the results and discussion section, oxidation of the substrate in the feed stream was negligible.

One experiment was performed in quadruplicate in order to assess the reproducibility of experimental data.

3. Results and discussion

3.1. REM characterization

The REM was characterized in order to anticipate its suitability for the removal of organic pollutants from water. SEM images presented in Fig. 2a and b show the uniform and interconnected structure of REM pores. Pore structure was further characterized by Hg porosimetry (Fig. 2c and d). Differential and cumulative intrusion pore volume indicate a mono-modal pore size distribution ranging between 0.8 and 1.9 μm with median pore diameter of 1.4 μm. Hg porosimetry analysis also determined a porous volume of 41% and specific surface area of 0.40 m^2 g^{-1}. These characteristics correspond to microfiltration membranes allowing the separation of particles and bacteria, while dissolved species pass through the membrane. The porous structure of the REM is tailored for reaching high permeate flux. Water permeability was determined as 3300 L m^{-2} h^{-1} bar^{-1}. This is 67-fold higher than commercial Ebonex® electrodes (Vector Corrosion Technologies, Inc.) consisting primarily of Ti_4O_7, which present a bimodal pore size distribution. While micro-sized pores range between 1 and 6 μm, nano-sized pores (<10 nm) strongly increase pressure drop across Ebonex® membranes (Zaky and Chaplin, 2013). Similar flux (3208 L m^{-2} h^{-1} bar^{-1}) was obtained by Guo et al. (2016) with TiO_2 membranes reduced to Ti_4O_7 using a thermal method at 1050 °C under 1 atm H_2 during 50 h (Guo et al., 2016). The median pore size diameter of these membranes was 2.99 μm, however, the 70 μm thick active layer with smaller pores could not be characterized by Hg

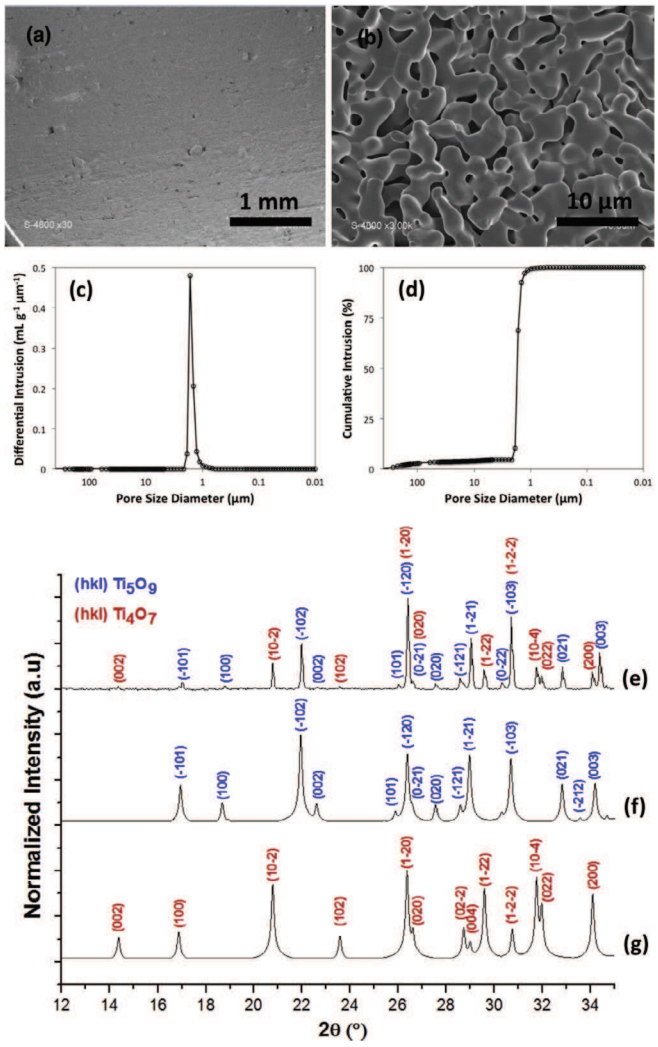

Fig. 2. Physico-chemical characteristics of the reactive electrochemical membrane (REM) Scanning electron microscopy of inner surface: (a) ×30, (b) ×3000. Data of Hg intrusion porosimetry analysis: (c) differential pore volume, (d) cumulative pore volume. X-ray diffraction data: (e) REM, (f) Ti_5O_9 (from Hodeau and Marezio (1979), (g) Ti_4O_7 (from Andersson and Jahnberg (1963).

porosimetry. Detailed study on limiting mechanisms for electro-oxidation showed three different behaviors according to permeate flux through the membrane (Zaky and Chaplin, 2013; Guo et al., 2016). Mass transport rate is the key parameter since electro-oxidation reactions occur at the membrane/pore surface. At low permeate flux and convection rate, diffusion can limit organic compound oxidation, similarly to conventional plane configurations (parallel plate electrodes). Convection-enhanced mass transport of pollutants is observed at higher permeate fluxes and the diffusion boundary layer is eliminated (Gao and Vecitis, 2012; Zaky and Chaplin, 2013). By continuously increasing the permeate flux, an ultimate limitation can finally arise from the electron transfer rate. This kinetic limitation depends on the nature of the substrate to oxidize, intrinsic kinetic reactivity of the REM and current supplied. From the comparison to values reported by Guo et al. (2016) with a similar configuration, it is anticipated that the high permeability of the REM used during this study avoid diffusion limitations during electro-oxidation of organic compounds, even at the lowest flux used (TMP = 40 mbar; J ≈ 120 L h^{-1} m^{-2}).

The electrochemical performance of REM also tightly depends on the nature of the Magnéli phase. Comparison of XRD data of the REM and TiO_x standards shows the presence of a mixture of Ti_4O_7 and Ti_5O_9 phases (Fig. 2e, f and 2g). None studies focused on the electrochemical performance of Ti_5O_9 for organic compound oxidation but the most conductive Magnéli phase is known to be Ti_4O_7 and recent studies demonstrated that this phase is able to produce $^{\bullet}OH$ from water oxidation (Guo et al., 2016; Ganiyu et al., 2016, 2017). Overall, physical characteristics of REM synthesized from carbothermal reduction of TiO_2 show that this material is tailored for water treatment applications, particularly for oxidation of organic pollutants. Moreover, this innovative synthesis method has the great advantage to reduce thermal treatment times and to avoid H_2 consumption.

3.2. Electrochemical oxidation of organic compounds

The efficiency of the REM for mineralization of organic molecules was assessed using various model compounds involving different electro-oxidation mechanisms. Hydroxyl radicals generated at the surface of a BDD anode are able to participate to the oxidation of OA (Martınez-Huitle et al., 2004; Garcia-Segura and Brillas, 2011). However, based on the very low absolute rate constant for the reaction of $^{\bullet}OH$ with OA - 1.4×10^6 M^{-1} s^{-1} (Weiss et al., 2007; Ferro et al., 2010) — Guo et al. (2016) considered that OA could be used as a direct oxidation probe. As regards to PHE and PCT, both DET and $^{\bullet}OH$ mediated oxidation can participate to the mineralization (rate constant of 1.4×10^{10} L mol^{-1} s^{-1} for oxidation of PCT by $^{\bullet}OH$ (Land and Ebert, 1967); rate constant of 9.8×10^9 L mol^{-1} s^{-1} for oxidation of PHE by $^{\bullet}OH$ (Bisby and Tabassum, 1988)). Besides, poisoning effect or anode fouling from electro-polymerization is often observed during electro-oxidation of PHE at the surface of anode materials with low O_2 overpotential, *i.e.* when oxidation mainly occurs by DET (Belhadj Tahar and Savall, 2009a, 2009b; Panizza and Cerisola, 2009).

Preliminary studies without current supply showed the absence of adsorption of these organic compounds in membrane pores and other parts of the pilot. It was also observed that oxidation mainly resulted from convection through the REM. Results from an electro-oxidation experiment at 30 mA cm^{-2} and TMP = 40 mbar during 90 min showed that >98% degradation and mineralization of 0.18 mM (TOC = 18 mg L^{-1}) of PCT was achieved in the permeate all along the experiment, while PCT and TOC concentration in the feed stream only decreased by 9% and <5% (after 90 min), respectively. Molecules oxidized at the outer surface of the REM are not accumulated in the retentate because back diffusion is low compared to forward convection (Gao and Vecitis, 2012). Thus, reaction in the feed stream was neglected, compared to the reaction through the REM. A quasi-permanent steady-state of both feed and permeate flux/concentration was reached few minutes after anodic polarization of the REM. Permeate was sampled until the same volume of solution was filtered (350 mL) for all experiments. Therefore, each data point reported in Figs. 3, 4 and 7b refers to a single experiment. The efficiency was calculated by comparing the concentration in the collected permeate and in the feed stream (considered as constant).

One experiment (TMP = 100 mbar; [PCT] = 0.33 mM; TOC = 32 mg L^{-1}; j = 15 mA cm^{-2}) was performed in quadruplicate in order to assess the reproducibility of experimental data. Low standard deviations were obtained for TOC flux (11.9 ± 0.4 g m^{-2} h^{-1}), percentage of TOC removal (60 ± 3%), TOC removal rate (7.1 ± 0.3 g m^{-2} h^{-1}) and MCE (49 ± 1%).

3.2.1. Oxidation of oxalic acid

Fig. 3 shows results obtained for the two-electron oxidation of OA to CO_2 and H_2O at 15 mA cm^{-2}. For example, 75% of TOC removal from a solution containing 354 mgC L^{-1} was achieved after a single passage through the membrane with a permeate flux of 139 L h^{-1} m^2 (TOC flux = 49 g h^{-1} m^{-2}). Results from increasing concentrations of oxalic acid (TMP = constant = 40 mbar) are compared with results from increasing TMP (C_f = constant = 18 mgC L^{-1}). An ultimate current limitation was drawn according to the maximum amount of electron that can be used for oxidation of OA (black solid lines in Fig. 3). This depends on the amount of electron supplied to the system (current density) and on the amount of OA available for oxidation (TOC flux).

Both OA concentration and permeate flux influences the TOC flux through the REM. When experiments were performed at the same TMP (40 mbar) and increasing OA concentrations (C_f = 18–800 mgC L^{-1}), TOC removal rate and MCE reached a plateau around 47 g m^{-2} h^{-1} and 72%, respectively, indicating that a kinetic limitation was reached. At relatively low OA flux (<30 g m^{-2} h^{-1}), almost full mineralization of OA was achieved. However, at the highest OA flux, the kinetic limitation observed for OA oxidation could not reach the ultimate current limitation (MCE = 100%). In fact, a portion of electrons is also consumed in oxygen evolution reactions *i.e* the generation of O_2 and $^{\bullet}OH$ that do not react or react slowly with OA. Maximum TOC removal rate of OA was 4.9-fold higher than the maximum reported in the literature using REM at a constant anodic potential of 2.94 V (47 *vs* 9.6 g m^{-2} h^{-1}), most probably because of the higher current density used in this study leading to an increase of the kinetic limit (Guo et al., 2016).

Different behavior was observed when experiments were performed at constant OA concentration (C_f = 18 mgC L^{-1}) and increasing TMP (*i.e.* increasing permeate flux). TOC removal rate and MCE of OA followed a bell curve with maximum of 14 g m^{-2} h^{-1} and 21% achieved for a TOC flux of 29 g m^{-2} h^{-1} (J = 1650 L m^{-2} h^{-1}). Similarly to the behavior observed with increasing OA concentration, OA oxidation also reached a kinetic limit when increasing the permeate flux. The difference actually lies in the increase of oxygen evolution reactions. High permeate fluxes increased O_2 gas bubbles sweeping from the REM surface, thus resulting in the promotion of the competitive reaction of oxygen evolution. Guo et al. (2016) reported the same behavior in a cross-flow filtration configuration using TiO_x REM from thermal reduction of TiO_2 under H_2. Lower TOC removal rate (9.6 g m^{-2} h^{-1}) but higher MCE (84%) was achieved for an optimal value of OA flux of 13.5 g m^{-2} h^{-1} (J = 561 L m^{-2} h^{-1}). Lower TOC removal rate and optimal value of permeate flux is ascribed to the lower current density (lower electron transfer rate). However, higher maximum MCE was reached because O_2 gas bubbles generation and sweeping

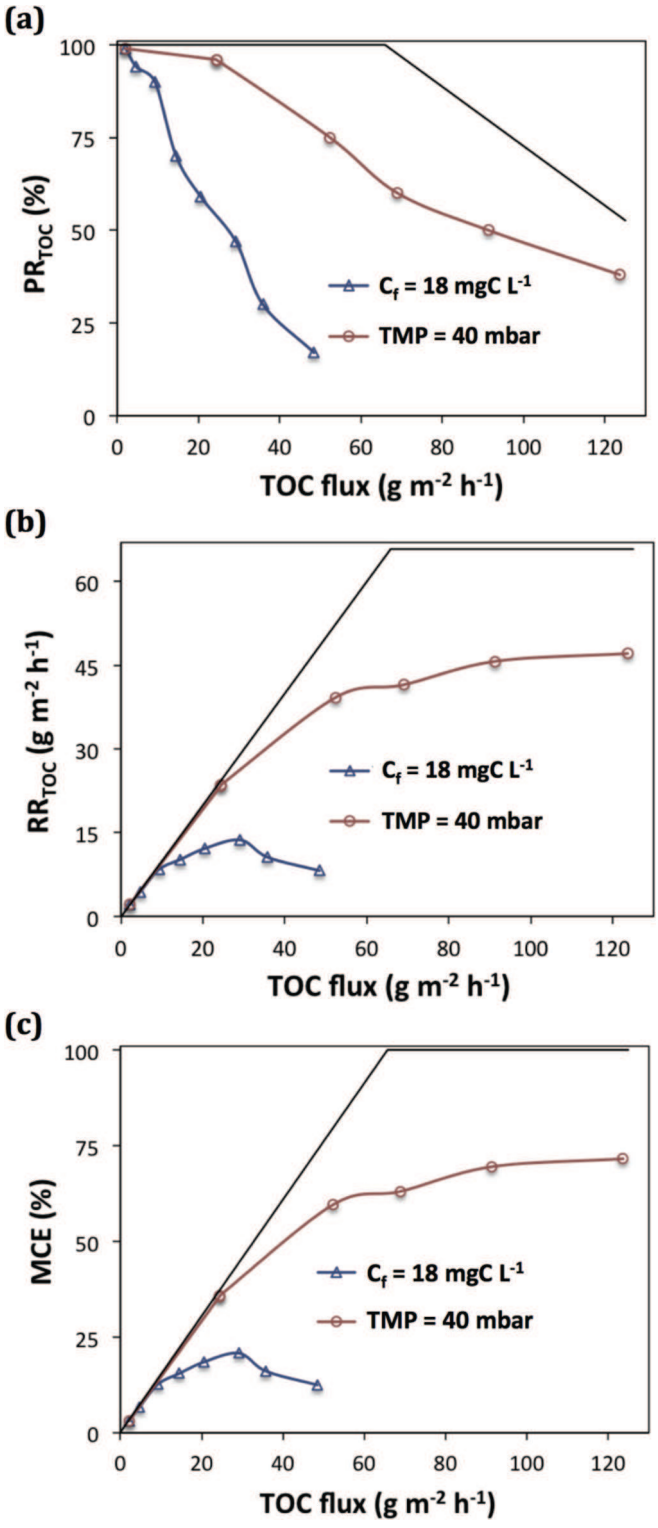

Fig. 3. Efficiency of oxalic acid removal from water by anodic oxidation on reactive electrochemical membrane as a function of total organic carbon (TOC) flux through the membrane: (a) percentage of TOC removal (PR_{TOC}), (b) TOC removal rate (RR_{TOC}), (c) mineralization current efficiency (MCE). Results from increasing concentrations of oxalic acid (TMP = constant = 40 mbar) are compared with results from increasing TMP (C_f = constant = 18 mgC L^{-1}). j = 15 mA cm^{-2}; $[Na_2SO_4]$ = 50 mM. Solid lines represent piece-wise interpolation and are included for easier reading of the figure. Black solid lines represent the ultimate current limitation, based on the maximum amount of electron that can be consumed for oxidation of OA.

was reduced because of the lower current density and lower optimal value of permeate flux, respectively.

3.2.2. Oxidation of paracetamol

PCT is an interesting model organic pollutant because both DET and •OH mediated oxidation is required in order to achieve efficient mineralization of the molecule. On one hand, PCT presents a high rate constant for oxidation by •OH (9.8×10^9 L mol^{-1} s^{-1}) and the well-known degradation by-product 1,4-benzoquinone is strongly refractory to DET (Brillas et al., 2005). On the other hand, OA and some other short-chain carboxylic acids generated as organic intermediates have lower oxidation rate by •OH and faster mineralization can be achieved by DET (Weiss et al., 2007).

The efficiency of PCT degradation and mineralization by the REM is shown in Fig. 4. Very high degradation rate of PCT was obtained, e.g. >99.9% degradation of PCT was reported until TOC flux reach 7, 14 and 20 g m^{-2} h^{-1} at 6, 15 and 30 mA cm^{-2}, respectively. However, higher efficiency was observed at high concentration/low TMP compared to experiments conducted at low concentration/high TMP. There is actually a competition between the reaction of free •OH with each other and with organic compounds (Kapałka et al., 2008). The dimerization reaction of •OH decreases mineralization efficiency through the consumption of •OH in non-organic events (scavenging reactions). Particularly, •OH dimerization has been observed to form hydrogen peroxide, and subsequently O_2 (Kapałka et al., 2009). Therefore, the increase of O_2 gas bubble sweeping at high permeate flux might lead to a shift of the equilibrium of these reactions and could promote the scavenging reactions of •OH dimerization.

Using PCT as model compound, the ultimate current limitation for TOC removal (by assuming MCE = 100%) is 5.7, 14.2 and 28.3 g m^{-2} h^{-1} at 6, 15 and 30 mA cm^{-2}, respectively. Compared to experiments with OA at the same current density (ultimate current limitation for TOC removal was 65.8 g m^{-2} h^{-1} at 15 mA cm^{-2}), a lower amount of TOC can be removed because more electrons are required to mineralize 1 mole of carbon (4.6 moles of e^- per mole of C for PCT and 1 mole of e^- per mole of C for OA).

When experiments were performed at the same TMP (40 mbar) and increasing PCT concentrations (C_f = 18–220 mgC L^{-1}), TOC removal rate and MCE did not reached a plateau; bell curves were observed and maximum MCE were reached for TOC flux around 5 (MCE = 49%), 8 (MCE = 47%) and 16 g m^{-2} h^{-1} (MCE = 43%) at 6, 15 and 30 mA cm^{-2}, respectively. Much higher MCE was obtained compared to a previous study using boron-doped diamond plate electrode (Brillas et al., 2005). The highest maximum TOC removal rate was obtained at high current density (12 g m^{-2} h^{-1} at 30 mA cm^{-2}) because of the increase of the electron transfer rate. However, the different bell curves obtained for the MCE at different current density clearly overlapped, meaning that the current density has to be adapted to the concentration of PCT in order to achieve maximum MCE. A dark-orange color was also observed in the permeate for experiments performed with operating conditions corresponding to the downward phase of the bell curve. The decrease of oxidation efficiency at high PCT concentration can be explained by taking into consideration the different oxidation mechanisms occurring in the REM according to the depth into the porous electrode. Jing et al. (2016) provided an approximation of the potential distribution in an ultrafiltration TiO_x REM, based on the analytical solution developed by Lasia (2008). The resistance of the electrode material and the concentration polarization of electroactive species were neglected. The main parameters influencing the calculation were pore radius, specific solution resistance, exchange current density and overpotential. The simulation showed that the potential dramatically drops in a cylindrical pore and reaches a value below the one required for •OH production at the

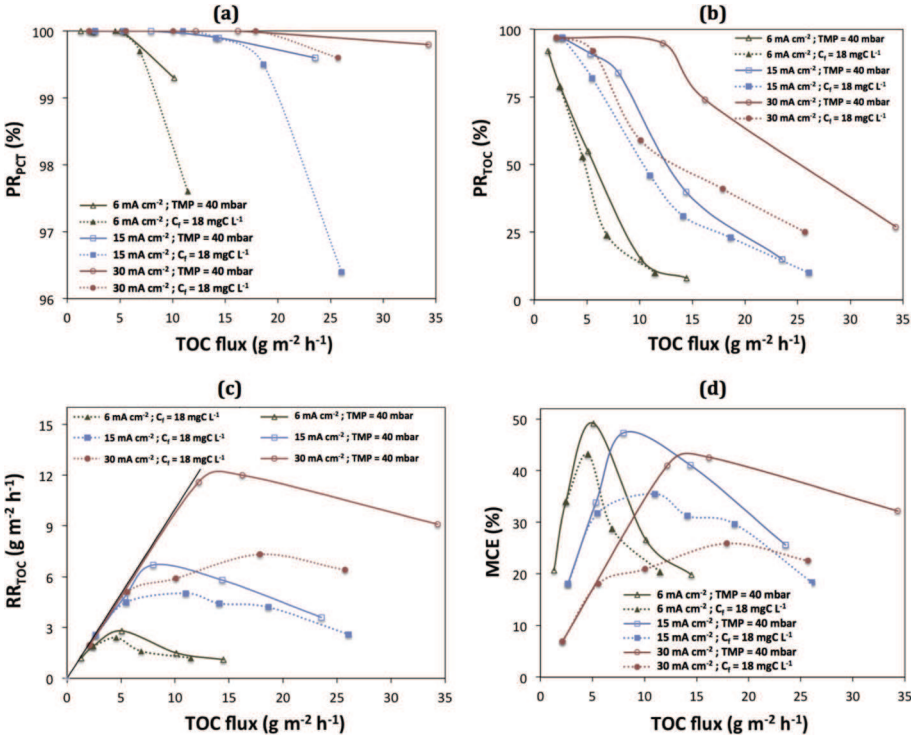

Fig. 4. Efficiency of paracetamol (PCT) removal from water by anodic oxidation on reactive electrochemical membrane as a function of total organic carbon (TOC) flux through the membrane and current density: (a) percentage of PCT removal (PR_{PCT}), (b) percentage of TOC removal (PR_{TOC}) (c) TOC removal rate (RR_{TOC}), (d) mineralization current efficiency (MCE). Results from increasing concentrations of PCT (TMP = constant = 40 mbar) are compared with results from increasing transmembrane pressure (TMP) (C_f = constant = 18 mgC L^{-1}). Experiments have been performed at 6, 15 and 30 mA cm^{-2}. $[Na_2SO_4]$ = 50 mM. Solid and dotted lines represent piece-wise interpolation and are included for easier reading of the figure.

depth of 0.023 μm. Below this potential, DET mainly occurs. Deeper into the membrane, the surface of the REM is not even anymore electro-active. DET is not able to achieve efficient mineralization of PCT: production of soluble dark-orange polymers was observed during the electro-oxidation of PCT on a Pt anode (active anode with low production of •OH) (Brillas et al., 2005) and PCT by-products identified in previous studies (Almeida et al., 2011; Feng et al., 2013) such as 1,4-benzoquinone are strongly refractory to DET. Therefore, bell curves observed during our experiments can be explained by the fact that •OH generated in the top layer of the REM are not sufficient to degrade all PCT molecules when the PCT concentration is too high. Thus, the MCE decreases due to electro-polymerization of PCT and presence of organic compounds recalcitrant to DET in the deeper REM layer where only DET occurs. On the contrary, maximum MCE is reached when PCT molecules are degraded by •OH to intermediate products highly reactive to DET, e.g. short-chain carboxylic acids such as OA.

When experiments were performed at the same PCT concentration (C_f = 18 mgC L^{-1}) and increasing TMP (40–470 mbar), similar phenomenon occurred. Thus, the results presented in this study show that the increase of the current density is required for maintaining elevated MCE during the treatment of high pollutant concentration or permeate flux (i.e. high TOC flux) because it allows avoiding the presence of organic compounds recalcitrant to DET in the layer where only DET occurs. Besides, lower oxidation efficiency was obtained during experiments conducted at high TMP compared to experiments at low TMP because of the enhancement of adverse effects coming from O_2 gas bubble sweeping, as described previously. This behavior is strongly enhanced at high current density because the optimal value of TOC flux is reached at higher permeate flux due to the increase of the electron transfer rate. However, the upward phase of bell curves observed during theses experiments shows that the efficiency of the electro-oxidation process for the removal of low concentration of organic compounds can be strongly improved by increasing the permeate flux to an optimal value, thanks to the increase of the convective mass transport of organic pollutants towards the anode surface.

A schematic view of the main phenomena involved in the electro-oxidation of organic pollutants is provided in Fig. 6.

A particular attention was also given to the evolution of the permeate flux during experiments performed at 30 mA cm^{-2} (Fig. 5). Using only the supporting electrolyte, permeate flux was observed to increase during the first 3–5 min of filtration due to the electro-osmotic flow. The electric field results in enhanced bulk liquid motion due to the net surplus of ions in the diffuse part of the electrical double layer formed at the surface of charged pores (Bowen and Clark, 1984; Huisman et al., 1998). This effect decreases at lower current density. Then, the permeate flux dropped around 65% of the initial water flux, followed by a period of stabilization (or slight decrease) between 10 and 90 min. The release of O_2 bubbles in the bulk from oxygen evolution at the anode reduces the liquid bulk volume active for filtration. In filtration mode, O_2 gas bubbles are continuously swept from the anode surface and a steady state is reached between the amount of O_2 produced and flushed out from the REM. When current was not anymore supplied, the permeate flux was restored to its initial value in 20 min, once all O_2 gas bubbles were flushed out. Very similar behavior was observed using low concentration of PCT. The permeate flux was restored to its initial value and none permeability loss was observed even after several successive experiments. At high concentration of PCT, the

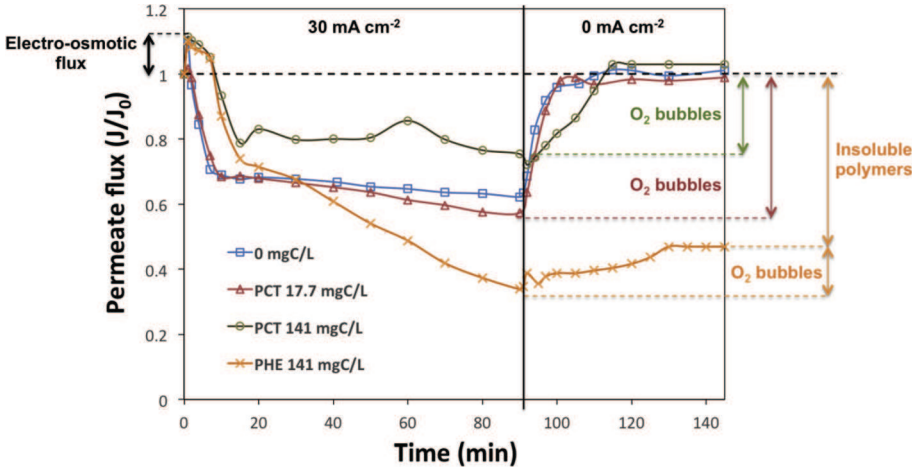

Fig. 5. Evolution of the permeate flux during the treatment of paracetamol (PCT) at 17.7 mgC L^{-1} or 141 mgC L^{-1}, phenol (PHE) at 141 mgC L^{-1} and in the absence of organic compound. Current density is set at 30 mA cm^{-2} during 90 min, then, none current was supplied during 50 min [Na_2SO_4] = 50 mM. Solid lines represent piece-wise interpolation and are included for easier reading of the figure.

drop of the permeate flux was slower and stabilized around 80% of the initial flux, indicating a lower production rate of O_2 gas bubbles. In fact, the increase of the concentration of PCT favors the reaction of •OH with organic compounds and hinders the reaction of •OH dimerization as well as subsequent reactions leading to the formation of O_2 (Fig. 6). Besides, PCT may also increase the overpotential of oxygen evolution, which inhibited the reaction of oxygen evolution. Further electrochemical characterizations would be required in order to clarify the explanation of this phenomenon. The evolution of the permeate flux was also observed to depend on the current density (data not shown). The higher the current density, the higher the drop of the permeate flux because of the increase of oxygen evolution reaction and generation of a greater amount of O_2 bubbles.

3.2.3. Phenol electro-oxidation

Different results were observed during electro-oxidation of PHE. Permeate flux continuously decreased during the whole experiment and could not be restored to its initial value when current was not anymore supplied. Permeability loss of the REM after 90 min of electro-oxidation is reported in Table 1, according to PHE concentration and current density. REM fouling observed during the treatment of PHE with a high ratio between the PHE concentration and the current density can be explained by taking into account similar electro-oxidation mechanisms than those reported in this study for PCT. When the concentration of PHE is too high with respect to the current supplied, •OH produced in the top layer of the REM are not sufficient to oxidize all PHE molecules. Therefore PHE and degradation by-products can react in the deeper reactive layer

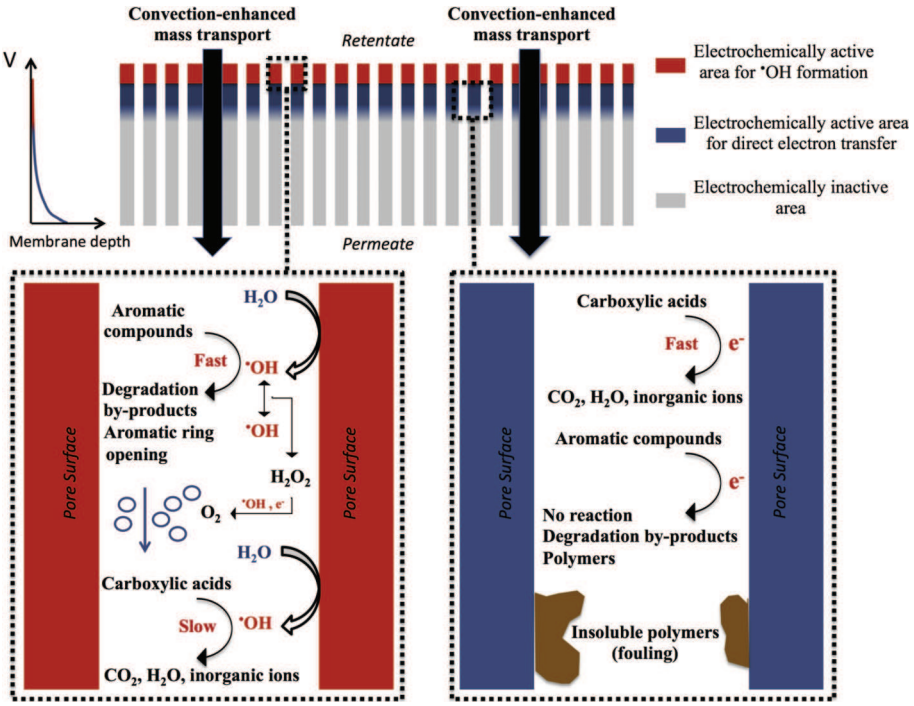

Fig. 6. Recapitulative scheme of the main electro-oxidation mechanisms of organic compounds in the reactive electrochemical membrane.

Table 1
Summary and comparison of results obtained for the treatment of paracetamol (PCT) and phenol (PHE) at different concentration and current density. Percentage of TOC removal (PR_{TOC}) of organic pollutants and permeability loss after the experiment have been assessed. All experiments have been performed during 90 min at TMP = 40 mbar.

Pollutant	C (mgC L^{-1})	j (mA cm^{-2})	PR_{TOC} (%)	Permeability loss (%)
PCT	17.7	6	79	<3
PCT	141	30	74	<3
PHE	17.7	6	94	9
PHE	35.5	6	76	13
PHE	141	6	38	17
PHE	17.7	30	>98	<3
PHE	35.5	30	>98	<3
PHE	141	30	95	53

by DET (Fig. 6). While such reaction has been observed to form soluble dark-orange polymers with PCT (Brillas et al., 2005), it has been widely reported that direct oxidation of PHE at the anode surface lead to the formation of insoluble polymers strongly interacting with the anode surface (Belhadj Tahar and Savall, 2009a; Gao and Vecitis, 2013). Thus, adsorption of polymers led to high percentage of TOC removal and high TOC removal rate of PHE, because large amounts of organic compounds (polymers) were physically retained within the membrane. However, these polymeric films cannot be mineralized. The adsorption of these polymers is responsible of pore blocking or pore size reduction (Fig. 6), which results in the irreversible decrease of the REM permeability. At both high current density and high PHE concentration, permeability loss reached its highest level because a greater amount of DET reactions occurred between the pore surface of the deep reactive layer and non- or hardly degraded PHE molecules. However, it was observed that it is possible to avoid REM fouling when performing experiments with a sufficiently high current density with respect to the concentration of PHE (Table 1). The aim is to reach a high mineralization degree and rate of PHE in the top layer of the REM where $^{\bullet}OH$ are produced in order to avoid direct oxidation of PHE and other aromatic by-products in the deep reactive layer where only DET occurs.

3.2.4. Evolution of the pH

The evolution of the pH was monitored both in the permeate and in the retentate (Fig. 7a). During an experiment at 30 mA cm^{-2} and [PCT] = 0.18 mM, it was observed a rapid increase of the pH in the retentate (11.1 at t = 10 min; 11.8 at t = 30 min), followed by a period of slow increase (12.2 at t = 90 min). In the permeate, pH rapidly reached a stable value around 1.8. When the feed water is passing through the membrane, H^+ generated from water oxidation at the anode (eq. (2)) are accumulated in the permeate due to the convective mass transport. On the contrary, OH^- generated at the cathode (stainless steel rod) are accumulated in the retentate. Stabilized values of pH observed in the permeate according to operating conditions are plotted in Fig. 7b pH was mainly affected by current density and permeate flux. During experiments with PCT as model organic compounds, pH in the permeate ranged between 1.8 and 3.2 according to operating conditions. Lowest pH was observed at high current density (high amount of H^+ generated) and low permeate flux (low dilution of generated H^+). Further investigations would be required in order to emphasize the influence of this pH gradient on electro-oxidation mechanisms and efficiency.

4. Conclusion

Unprecedented high efficiency of mineralization of organic compounds is presented in this study by using an innovative REM

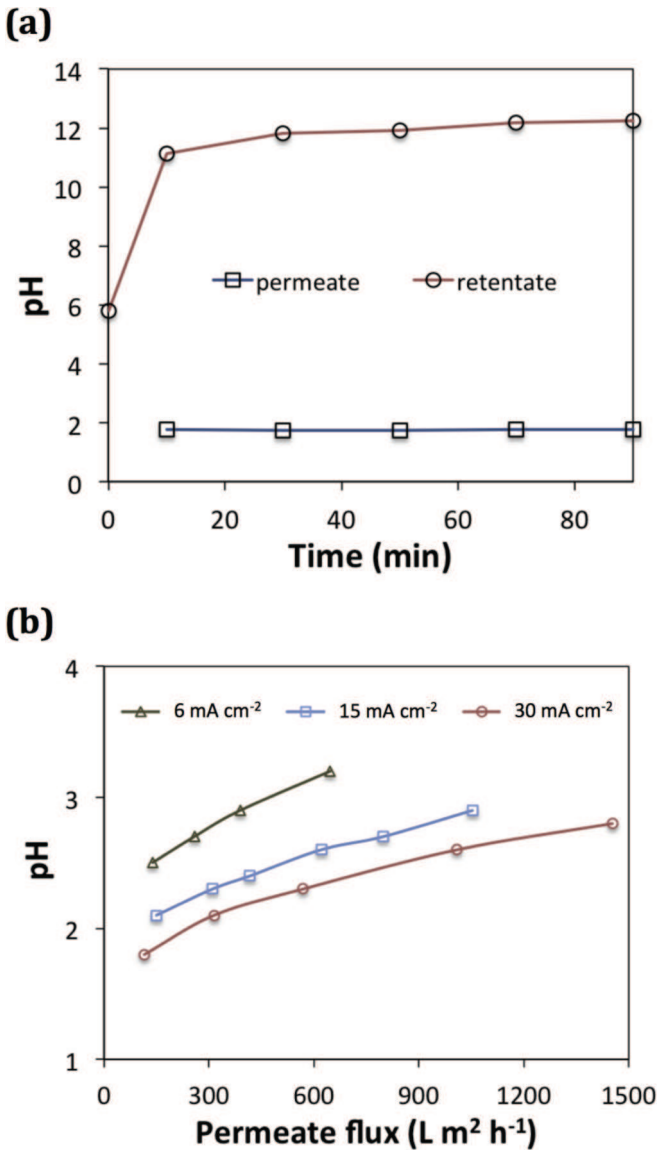

Fig. 7. (a) Evolution of the pH in the permeate and in the retentate during the treatment of paracetamol (PCT) at 0.18 mM (j = 30 mA cm^{-2}; J = 110 L h^{-1} m^{-2}). (b) Stabilized value of pH in the permeate according to current density and permeate flux ([PCT] = 0.18 mM).

synthesized from carbothermal reduction of TiO_2. The homogeneous pore structure (median pore size = 1.4 μm) and suitable Magnéli phase synthesized (mixture of Ti_4O_7 and Ti_5O_9) resulted in high permeability (3300 L h^{-1} m^{-2}), high convection-enhanced mass transfer and excellent reactivity of the REM. From the high TOC removal rates (6.7 g m^{-2} h^{-1} and 47 g m^{-2} h^{-1} for PCT and OA, respectively, at 15 mA cm^{-2}) and mineralization current efficiency (47% and 72% for PCT and OA, respectively, at 15 mA cm^{-2}) achieved, the great promise of this new water treatment technology has been emphasized. Two limitations have been also highlighted. A decrease of the process efficiency has been observed at high TOC flux due to the effect of the decrease of the anodic potential according to the REM depth. Hydroxyl radicals can be only generated in the top layer of the REM. Therefore, adverse effects arises from the presence of refractory organic compounds and from electropolymerization in the deeper layer where only DET occurs. In the case of PHE, interaction of electro-generated polymers with the

pore surface strongly reduced the membrane permeability (fouling). Besides, at high permeate flux, a decrease of the electro-oxidation efficiency was observed due to enhanced sweeping of O_2 bubbles from the anode surface, which promotes oxygen evolution reactions. Whatever the organic compound studied, current density appeared as the crucial parameter for limiting these adverse effects. Fortunately, the advantage of electro-oxidation is the possibility to easily tune current intensity in order to adapt the process to effluent concentration and/or permeate flux. While the efficiency of the REM was observed to be constant during this study, the assessment of the long-term lifetime of these electrodes is the focus of ongoing research in order to confirm the suitability of this process for water treatment. Then, the use of REM for the treatment of real effluents will be investigated since particles and colloids in real water matrix may affect the efficiency of the process.

Acknowledgment

We gratefully acknowledge the National French Agency of Research 'ANR' for funding the project ECO-TS/CElectrON (ANR-13-ECOT-003). Clément Trellu particularly thanks the agency for post-doctoral fellowship. Authors are also grateful to Saint Gobain CREE for supplying reactive electrochemical membranes in the framework of the ANR program.

References

Almeida, L.C., Garcia-Segura, S., Bocchi, N., Brillas, E., 2011. Solar photoelectro-Fenton degradation of paracetamol using a flow plant with a Pt/air-diffusion cell coupled with a compound parabolic collector: process optimization by response surface methodology. Appl. Catal. B Environ. 103, 21–30. https://doi.org/10.1016/j.apcatb.2011.01.003.

Andersson, S., Jahnberg, L., 1963. Crystal structure studies on the homologous series TinO2n-1, VnO2n-1, Tin-2Cr2O2n-1. Ark. Foer Kemi 21, 423–426.

Antonin, V.S., Santos, M.C., Garcia-Segura, S., Brillas, E., 2015. Electrochemical incineration of the antibiotic ciprofloxacin in sulfate medium and synthetic urine matrix. Water Res. 83, 31–41. https://doi.org/10.1016/j.watres.2015.05.066.

Balci, B., Oturan, N., Cherrier, R., Oturan, M.A., 2009. Degradation of atrazine in aqueous medium by electrocatalytically generated hydroxyl radicals. A kinetic and mechanistic study. Water Res. 43, 1924–1934. https://doi.org/10.1016/j.watres.2009.01.021.

Belhadj Tahar, N., Savall, A., 2009a. Electrochemical removal of phenol in alkaline solution. Contribution of the anodic polymerization on different electrode materials. Electrochim. Acta 54, 4809–4816. https://doi.org/10.1016/j.electacta.2009.03.086.

Belhadj Tahar, N., Savall, A., 2009b. Electropolymerization of phenol on a vitreous carbon electrode in alkaline aqueous solution at different temperatures. Electrochimica Acta. In: Electrochemistry with Spatial and Temporal Resolution Selection of Papers from the 4th Gerischer Symposium 25-27 June 2008, Berlin, Germany, vol. 55, pp. 465–469. https://doi.org/10.1016/j.electacta.2009.08.040.

Bisby, R.H., Tabassum, N., 1988. Properties of the radicals formed by one-electron oxidation of acetaminophen—a pulse radiolysis study. Biochem. Pharmacol. 37, 2731–2738. https://doi.org/10.1016/0006-2952(88)90035-4.

Bowen, W.R., Clark, R.A., 1984. Electro-osmosis at microporous membranes and the determination of zeta-potential. J. Colloid Interface Sci. 97, 401–409. https://doi.org/10.1016/0021-9797(84)90311-4.

Brillas, E., Martínez-Huitle, C.A., 2015. Decontamination of wastewaters containing synthetic organic dyes by electrochemical methods. An updated review. Appl. Catal. B Environ. 166–167, 603–643. https://doi.org/10.1016/j.apcatb.2014.11.016.

Synthetic diamond films. In: Brillas, E., Martínez-Huitle, C.A. (Eds.), 2011. Preparation, Electrochemistry, Characterization, and Applications. John Wiley & Sons, Inc., Hoboken, NJ, USA.

Brillas, E., Sirés, I., Arias, C., Cabot, P.L., Centellas, F., Rodríguez, R.M., Garrido, J.A., 2005. Mineralization of paracetamol in aqueous medium by anodic oxidation with a boron-doped diamond electrode. Chemosphere 58, 399–406. https://doi.org/10.1016/j.chemosphere.2004.09.028.

Brillas, E., Sirés, I., Oturan, M.A., 2009. Electro-Fenton process and related electrochemical technologies based on Fenton's reaction chemistry. Chem. Rev. 109, 6570–6631. https://doi.org/10.1021/cr900136g.

Chaplin, B.P., 2014. Critical review of electrochemical advanced oxidation processes for water treatment applications. Environ. Sci. Process. Impacts. https://doi.org/10.1039/C3EM00679D.

Feng, L., van Hullebusch, E.D., Rodrigo, M.A., Esposito, G., Oturan, M.A., 2013. Removal of residual anti-inflammatory and analgesic pharmaceuticals from aqueous systems by electrochemical advanced oxidation processes. A review. Chem. Eng. J. 228, 944–964. https://doi.org/10.1016/j.cej.2013.05.061.

Ferro, S., Martínez-Huitle, C.A., Battisti, A.D., 2010. Electrooxidation of oxalic acid at different electrode materials. J. Appl. Electrochem. 40, 1779–1787. https://doi.org/10.1007/s10800-010-0113-y.

Ganiyu, S.O., Oturan, N., Raffy, S., Cretin, M., Esmilaire, R., van Hullebusch, E., Esposito, G., Oturan, M.A., 2016. Sub-stoichiometric titanium oxide (Ti4O7) as a suitable ceramic anode for electrooxidation of organic pollutants: a case study of kinetics, mineralization and toxicity assessment of amoxicillin. Water Res. 106, 171–182. https://doi.org/10.1016/j.watres.2016.09.056.

Ganiyu, S.O., Oturan, N., Raffy, S., Esposito, G., van Hullebusch, E.D., Cretin, M., Oturan, M.A., 2017. Use of sub-stoichiometric titanium oxide as a ceramic electrode in anodic oxidation and electro-fenton degradation of the beta-blocker propranolol: degradation kinetics and mineralization pathway. Electrochim. Acta 242, 344–354. https://doi.org/10.1016/j.electacta.2017.05.047.

Ganiyu, S.O., van Hullebusch, E.D., Cretin, M., Esposito, G., Oturan, M.A., 2015. Coupling of Membrane Filtration and Advanced Oxidation Processes for Removal of Pharmaceutical Residues: a Critical Review. Sep. Purif. Technol., Environmental Nanotechnology and Sustainability in Water Treatment in Honor of Professor Chin-pao Huang, Ph.D, Harvard University, Donald C. Philips, Professor Civil and Environmental Engineering, University of Delaware, USA 156, Part 3, pp. 891–914. https://doi.org/10.1016/j.seppur.2015.09.059.

Gao, G., Vecitis, C.D., 2013. Electrocatalysis aqueous phenol with carbon nanotubes networks as anodes: electrodes passivation and regeneration and prevention. Electrochim. Acta 98, 131–138. https://doi.org/10.1016/j.electacta.2013.02.127.

Gao, G., Vecitis, C.D., 2012. Reactive depth and performance of an electrochemical carbon nanotube network as a function of mass transport. ACS Appl. Mater. Interfaces 4, 6096–6103. https://doi.org/10.1021/am301724n.

Garcia-Segura, S., Brillas, E., 2011. Mineralization of the recalcitrant oxalic and oxamic acids by electrochemical advanced oxidation processes using a boron-doped diamond anode. Water Res. 45, 2975–2984. https://doi.org/10.1016/j.watres.2011.03.017.

Guo, L., Jing, Y., Chaplin, B.P., 2016. Development and characterization of ultrafiltration TiO2 Magnéli phase reactive electrochemical membranes. Environ. Sci. Technol. 50, 1428–1436. https://doi.org/10.1021/acs.est.5b04366.

Hodeau, J.L., Marezio, M., 1979. Structural aspects of the metal-insulator transitions in (Ti0.9975V0.0025)4O7. J. Solid State Chem. 29, 47–62. https://doi.org/10.1016/0022-4596(79)90208-1.

Huisman, I.H., Trägårdh, G., Trägårdh, C., Pihlajamäki, A., 1998. Determining the zeta-potential of ceramic microfiltration membranes using the electroviscous effect. J. Membr. Sci. 147, 187–194. https://doi.org/10.1016/S0376-7388(98)00135-5.

Jing, Y., Guo, L., Chaplin, B.P., 2016. Electrochemical impedance spectroscopy study of membrane fouling and electrochemical regeneration at a sub-stoichiometric TiO2 reactive electrochemical membrane. J. Membr. Sci. 510, 510–523. https://doi.org/10.1016/j.memsci.2016.03.029.

Kapałka, A., Fóti, G., Comninellis, C., 2009. The importance of electrode material in environmental electrochemistry: formation and reactivity of free hydroxyl radicals on boron-doped diamond electrodes. Electrochimica Acta. In: Electrochemistry for a HEALTHY Planetenvironmental Analytical and Engineering Aspects Selection of Papers from the 6th ISE Spring Meeting 16–19 March 2008, Foz do Iguaçu, Brazil, vol. 54, pp. 2018–2023. https://doi.org/10.1016/j.electacta.2008.06.045.

Kapałka, A., Fóti, G., Comninellis, C., 2008. Kinetic modelling of the electrochemical mineralization of organic pollutants for wastewater treatment. J. Appl. Electrochem. 38, 7–16. https://doi.org/10.1007/s10800-007-9365-6.

Land, E.J., Ebert, M., 1967. Pulse radiolysis studies of aqueous phenol. Water elimination from dihydroxycyclohexadienyl radicals to form phenoxyl. Trans. Faraday Soc. 63, 1181–1190. https://doi.org/10.1039/TF9676301181.

Lasia, A., 2008. Modeling of impedance of porous electrodes, in: modeling and numerical simulations, modern aspects of electrochemistry. Springer New York 67–137. https://doi.org/10.1007/978-0-387-49582-8_3.

Latimer, W.M., 1952. Oxidation Potentials. Prentice-Hall.

Liu, Y., Liu, H., Zhou, Z., Wang, T., Ong, C.N., Vecitis, C.D., 2015. Degradation of the common aqueous antibiotic tetracycline using a carbon nanotube electrochemical filter. Environ. Sci. Technol. 49, 7974–7980. https://doi.org/10.1021/acs.est.5b00870.

Martínez-Huitle, C.A., Rodrigo, M.A., Sirés, I., Scialdone, O., 2015. Single and coupled electrochemical processes and reactors for the abatement of organic water pollutants: a critical review. Chem. Rev. 115, 13362–13407. https://doi.org/10.1021/acs.chemrev.5b00361.

Martínez-Huitle, C.A., Ferro, S., De Battisti, A., 2004. Electrochemical incineration of oxalic acid: role of electrode material. Electrochimica Acta. The role of electrochemistry in the sustained development of modern societies 49, 4027–4034. https://doi.org/10.1016/j.electacta.2004.01.083.

Moreira, F.C., Boaventura, R.A.R., Brillas, E., Vilar, V.J.P., 2017. Electrochemical advanced oxidation processes: a review on their application to synthetic and real wastewaters. Appl. Catal. B Environ. 202, 217–261. https://doi.org/10.1016/j.apcatb.2016.08.037.

Oturan, N., van Hullebusch, E.D., Zhang, H., Mazeas, L., Budzinski, H., Le Menach, K., Oturan, M.A., 2015. Occurrence and removal of organic micropollutants in landfill leachates treated by electrochemical advanced oxidation processes. Environ. Sci. Technol. 49, 12187–12196. https://doi.org/10.1021/acs.est.5b02809.

Özcan, A., Sahin, Y., Koparal, A.S., Oturan, M.A., 2008. Propham mineralization in aqueous medium by anodic oxidation using boron-doped diamond anode:

influence of experimental parameters on degradation kinetics and mineralization efficiency. Water Res. 42, 2889–2898. https://doi.org/10.1016/j.watres.2008.02.027.
Panizza, M., Cerisola, G., 2009. Direct and mediated anodic oxidation of organic pollutants. Chem. Rev. 109, 6541–6569. https://doi.org/10.1021/cr9001319.
Panizza, M., Michaud, P.A., Cerisola, G., Comninellis, C., 2001. Anodic oxidation of 2-naphthol at boron-doped diamond electrodes. J. Electroanal. Chem. 507, 206–214. https://doi.org/10.1016/S0022-0728(01)00398-9.
Radjenovic, J., Sedlak, D.L., 2015. Challenges and opportunities for electrochemical processes as next-generation technologies for the treatment of contaminated water. Environ. Sci. Technol. 49, 11292–11302. https://doi.org/10.1021/acs.est.5b02414.
Ronen, A., Walker, S.L., Jassby, D., 2016. Electroconductive and electroresponsive membranes for water treatment. Rev. Chem. Eng. 32. https://doi.org/10.1515/revce-2015-0060.
Schnoor, M.H., Vecitis, C.D., 2013. Quantitative examination of aqueous ferrocyanide oxidation in a carbon nanotube electrochemical filter: effects of flow rate, ionic strength, and cathode material. J. Phys. Chem. C 117, 2855–2867. https://doi.org/10.1021/jp3112099.
Trellu, C., Péchaud, Y., Oturan, N., Mousset, E., Huguenot, D., Hullebusch, E.D., van Esposito, G., Oturan, M.A., 2016. Comparative study on the removal of humic acids from drinking water by anodic oxidation and electro-Fenton processes: mineralization efficiency and modelling. Appl. Catal. B Environ. 194, 32–41. https://doi.org/10.1016/j.apcatb.2016.04.039.
Tsierkezos, N.G., Ritter, U., 2012. Electrochemical and thermodynamic properties of hexacyanoferrate(II)/(III) redox system on multi-walled carbon nanotubes. J. Chem. Therm. 54, 35–40. https://doi.org/10.1016/j.jct.2012.03.018.
Walsh, F.C., Wills, R.G.A., 2010. The continuing development of Magnéli phase titanium sub-oxides and Ebonex® electrodes. Electrochim. Acta 55, 6342–6351. https://doi.org/10.1016/j.electacta.2010.05.011.
Weiss, E., Groenen-Serrano, K., Savall, A., Comninellis, C., 2007. A kinetic study of the electrochemical oxidation of maleic acid on boron doped diamond. J. Appl. Electrochem. 37, 41–47. https://doi.org/10.1007/s10800-006-9212-1.
Yang, J., Wang, J., Jia, J., 2009. Improvement of electrochemical wastewater treatment through mass transfer in a seepage carbon nanotube electrode reactor. Environ. Sci. Technol. 43, 3796–3802. https://doi.org/10.1021/es8034285.
Zaky, A.M., Chaplin, B.P., 2014. Mechanism of p-substituted phenol oxidation at a Ti4O7 reactive electrochemical membrane. Environ. Sci. Technol. 48, 5857–5867. https://doi.org/10.1021/es5010472.
Zaky, A.M., Chaplin, B.P., 2013. Porous substoichiometric TiO2 anodes as reactive electrochemical membranes for water treatment. Environ. Sci. Technol. 47, 6554–6563. https://doi.org/10.1021/es401287e.